23PM3F-03

High-Frequency Asymptotic Analysis for Scattered Field by a Conducting Cylinder

Keiji Goto [#1], Le Hoang Loc [#]

[#] *Department of Communication Engineering, National Defense Academy*
Yokosuka, Kanagawa, Japan
[1] keigoto@nda.ac.jp

***Abstract*—In this study, we consider the high-frequency asymptotic analysis methods for the scattered field when a cylindrical wave is incident on a conducting circular cylinder. We derive the asymptotic solution applicable in each of the transition regions divided by the shadow boundary into the shadow and the lit side. The asymptotic solutions include a novel extended Pekeris caret function to which the second order term in the argument of the exponential in the integrand is added as compared with the Pekeris caret function including the UTD (uniform GTD) solution. By applying the residue theorem and the saddle point technique to the novel extended Pekeris caret function, we derive respectively the surface diffracted ray solution and the reflected geometrical ray solution which are effective exterior to the transition regions. The validity of the various asymptotic solutions derived here is confirmed by comparing with the exact solution.**

I. Introduction

The studies in the high-frequency scattering by a smooth convex cylinder have been important research subjects for a variety of applications in the area of the analysis of the radiation patterns of antennas mounted near an aircraft fuselage and the radar cross section [1]-[9].

Pathak [3] and Pathak et al. [4] considered about the problem of the scattered field by a perfectly conducting cylinder and proposed the UTD (uniform GTD) solution which is applicable in the transition region [3], [5] near the shadow boundary (SB) and reduces automatically to the Keller's GTD solution [1] exterior to the transition region.

In this study, we consider the high-frequency asymptotic analysis methods for the scattered field by a conducting circular cylinder applicable in the transition regions divided by the SB into the shadow and the lit side. We newly derive the asymptotic solutions including an extended Pekeris caret function applicable in the transition regions. The extended Pekeris caret function derived in this study is denoted by the representation to which the second order term in the argument of the exponential in the integrand is added as compared with the Pekeris caret function in [3], [5], [10]. We derive the surface diffracted ray solution and the reflected geometrical ray solution effective exterior to the transition region by applying the residue theorem and the saddle point technique [11] to the extended Pekeris caret function.

The validity of the various asymptotic solutions derived here is confirmed by comparing with the exact solution obtained from the eigenfunction expansion [5], [9].

II. Formulation and Integral Representation for the Scattered Field

Figure 1 shows a conducting circular cylinder with the radius of curvature a and the coordinate systems (x, y, z) and (ρ, ϕ). The circular cylinder and the magnetic line source are placed in parallel and are extended from $-\infty$ to $+\infty$ in the z-direction. In this study, we consider the magnetic-type scattering problem in which the scattered magnetic field has only the z-direction component.

The scattered magnetic field $H_z^d(\mathrm{P})$, arriving at the observation point $\mathrm{P}(\rho, \phi)$ from the counterclockwise direction without encircling the circular cylinder after radiated from the magnetic line source $\mathrm{Q}(\rho_0, \phi_0)$, can be given as follows [12]

$$H_z^d(\mathrm{P}) \sim H_{z,\mathrm{in}}(\mathrm{Q}_1)\exp(ik\ell)B(k)I(\xi, L)\left\{\frac{\exp(iks_2)}{\sqrt{s_2}}\right\} \quad (1)$$

$$H_{z,\mathrm{in}}(\mathrm{Q}_1) = \frac{i}{4}\sqrt{\frac{2}{\pi k s_1}}\exp\left[iks_1 - i\frac{\pi}{4}\right] \quad (2)$$

$$s_1 = \overline{\mathrm{QQ}_1} = \sqrt{{\rho_0}^2 - a^2}\,, \quad s_2 = \overline{\mathrm{Q}_2\mathrm{P}} = \sqrt{\rho^2 - a^2} \quad (3)$$

$$\ell = a\theta\,,\ \theta = |\phi - \phi_0| - \cos^{-1}\left(\frac{a}{\rho_0}\right) - \cos^{-1}\left(\frac{a}{\rho}\right) \quad (4)$$

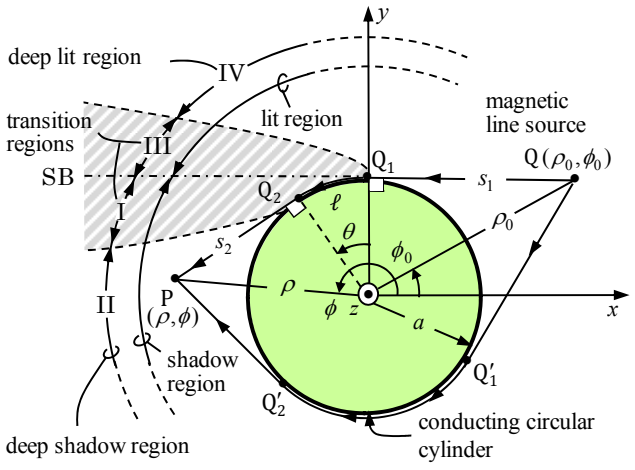

Fig. 1. Conducting circular cylinder, coordinate systems (x, y, z) and (ρ, ϕ), and schematic figure for surface diffracted ray. $\mathrm{Q}(\rho_0, \phi_0)$: magnetic line source. $\mathrm{P}(\rho, \phi)$: observation point. SB: shadow boundary.

$$B(k) = -M\sqrt{2/k}\ ,\ \ M = (ka/2)^{1/3}. \tag{5}$$

Here, $H_{z,\mathrm{in}}(\mathrm{Q}_1)$ denotes the incident ray propagating the distance from the source Q to the surface diffraction point Q_1 and ℓ the propagation distance from the point Q_1 to the other surface diffraction point Q_2 (see Fig. 1). The term in the brackets { } represents the cylindrical wave propagating the distance from the point Q_2 to the observation point P. Notation $I(\xi, L)$ denotes the transmission function, which expresses the scattering phenomena occurring along the arc ℓ and is defined as follows

$$I(\xi, L) = \frac{e^{-i\pi/4}}{2\sqrt{\pi}} \int_{-\infty}^{\infty} \frac{w_2'(t)}{w_1'(t)} \exp\left[i\xi t + i\frac{M^2}{2kL}t^2\right] dt \tag{6}$$

$$w_1'(t) = Ai'(t) - iBi'(t)\ ,\ \ w_2'(t) = Ai'(t) + iBi'(t) \tag{7}$$

$$\xi = M\theta\ (\geq 0)\ ,\quad L = s_1\, s_2/(\, s_1 + s_2). \tag{8}$$

Where $Ai(\cdot)$ and $Bi(\cdot)$ are the Airy functions [13] and the prime $(')$ on the functions denotes the derivative with respect to the argument. The time factor $\exp(-i\omega t)$ has been suppressed. In (1), the contribution from the direct ray before passing through a turning point when the observation point P is located to the lit region near the source Q has been omitted.

As shown in Fig. 1, the surrounding space of the conducting circular cylinder is separated by the SB into the shadow and the lit region. Furthermore, the shadow region is divided into the transition region I near the SB and the deep shadow region II. Similarly, the lit region is divided into the transition region III near the SB and the deep lit region IV.

III. High-Frequency Asymptotic Analysis for the Scattered Field

In this section, we consider the high-frequency asymptotic analysis methods for the scattered field applicable in the transition regions I and III near the SB. We also derive the surface diffracted ray solution in the deep shadow region III and the geometrical optics (GO) solution by the summation of the direct ray and the reflected geometrical ray in the deep lit region IV.

A. Asymptotic analysis in the transition region I

We consider an asymptotic analysis for the scattered field in the transition region I as shown in Fig. 1.

By applying the following relationship in the Airy function

$$w_2'(t) = 2Ai'(t) - w_1'(t) \tag{9}$$

into (6), the transmission function $I(\xi, L)$ can be given by

$$I(\xi, L) = I_0(\xi, L) + \hat{P}_h^{\mathrm{ext}}(\xi, L) \tag{10}$$

$$I_0(\xi, L) = -\frac{e^{-i\pi/4}}{2\sqrt{\pi}} \int_{-\infty}^{\infty} \exp\left[i\xi t + i\frac{M^2}{2kL}t^2\right] dt \tag{11}$$

$$\hat{P}_h^{\mathrm{ext}}(\xi, L) = \frac{e^{-i\pi/4}}{\sqrt{\pi}} \int_{-\infty}^{\infty} \frac{Ai'(t)}{w_1'(t)} \exp\left[i\xi t + i\frac{M^2}{2kL}t^2\right] dt\,. \tag{12}$$

When the integral $I_0(\xi, L)$ in (11) is performed by several manipulations, the following relationship can be obtained.

$$I_0(\xi, L) = \frac{e^{i\pi/4}}{2\xi\sqrt{\pi}}\left(i2Xe^{-iX^2}\sqrt{\pi}e^{i\pi/4}\right) \tag{13}$$

$$X = \sqrt{2kL}\theta/2\ \ (\geq 0). \tag{14}$$

The function $\hat{P}_h^{\mathrm{ext}}(\xi, L)$ in (12) differs in that the second order term including t^2 in the argument of the exponential in the integrand is added as compared with the conventional Pekeris caret function $\hat{P}_h(\xi)$ in [3], [5], [10]. Moreover, the function $\hat{P}_h^{\mathrm{ext}}(\xi, L)$ in (12) differs in the integration contour compared with the extended Pekeris caret function defined by [9]. In this study, we newly define the extended Pekeris caret function as $\hat{P}_h^{\mathrm{ext}}(\xi, L)$ in (12).

Dividing the integration interval $(-\infty, +\infty)$ in (12) into the two integration intervals $(-\infty, 0)$ and $(0, +\infty)$, and then performing the straightforward manipulation for the latter integral yield the following formula including the Fresnel function $F(X)$ [9], [12].

$$\hat{P}_h^{\mathrm{ext}}(\xi, L) = p_h^{\mathrm{ext}}(\xi, L) - \frac{e^{i\pi/4}}{2\xi\sqrt{\pi}}\left[i2Xe^{-iX^2}\sqrt{\pi}e^{i\pi/4} + F(X)\right] \quad \text{for } \xi \geq 0 \tag{15}$$

$$p_h^{\mathrm{ext}}(\xi, L) = \frac{e^{-i\pi/4}}{\sqrt{\pi}}\left[\int_0^{\infty} \frac{Ai'(t)}{w_1'(t)} \exp\left(i\xi t + i\frac{M^2}{2kL}t^2\right) dt + \int_0^{\infty} e^{i2\pi/3} \frac{Ai'(t)}{w_2'(t)} e^{-\xi t e^{i\pi/6} + \frac{M^2}{2kL}t^2 e^{-i\pi/6}} dt\right] \tag{16}$$

$$F(X) = -i2Xe^{-iX^2} \int_X^{\infty} e^{it^2} dt\ . \tag{17}$$

Substituting (13) and (15) into (10), the transmission function $I(\xi, L)$ can be represented by

$$I(\xi, L) = \frac{e^{i\pi/4}}{2\xi\sqrt{\pi}}\left(i2Xe^{-iX^2}\sqrt{\pi}e^{i\pi/4}\right) + \hat{P}_h^{\mathrm{ext}}(\xi, L) \tag{18}$$

and

$$I(\xi, L) = p_h^{\mathrm{ext}}(\xi, L) - \frac{e^{i\pi/4}}{2\xi\sqrt{\pi}}F(X)\,. \tag{19}$$

In this study, we newly define the extended Pekeris function as $p_h^{\mathrm{ext}}(\xi, L)$ in (16).

Substituting $I(\xi, L)$ in (18) into (1), one may obtain the following asymptotic solution for the scattered field applicable when the observation point is located in the transition region I ($\mathrm{P} = \mathrm{P_S}$):

$$H_z^d(\mathrm{P_S}) \sim H_{z,\,\mathrm{GO}}^{\mathrm{pseudo}}(\mathrm{P_S}) + H_{z,\mathrm{in}}(\mathrm{Q_1}) e^{ika\theta} B(k)\, \hat{P}_h^{\mathrm{ext}}(\xi, L) \frac{\exp(iks_2)}{\sqrt{s_2}} \quad (20)$$

where $H_{z,\,\mathrm{GO}}^{\mathrm{pseudo}}(\mathrm{P_S})$ is an pseudo incident wave which penetrates a conducting cylinder from the source Q and reaches the observation point $\mathrm{P_s}$ (see Fig. 2), and is given by

$$H_{z,\,\mathrm{GO}}^{\mathrm{pseudo}}(\mathrm{P_S}) = \frac{i}{4}\sqrt{\frac{2}{\pi k \bar{L}_0}} \exp\left[ik\bar{L}_0 - i\frac{\pi}{4}\right],\ \bar{L}_0 = \overline{\mathrm{QP_S}}\,. \quad (21)$$

In derivation of (21), the following approximations are used for the amplitude and the phase terms:

$$s_1 + s_2 \doteqdot \bar{L}_0 \quad \text{for the amplitude term} \quad (22)$$

$$s_1 + s_2 + a\theta - L\theta^2/2 \doteqdot \bar{L}_0 \quad \text{for the phase term.} \quad (23)$$

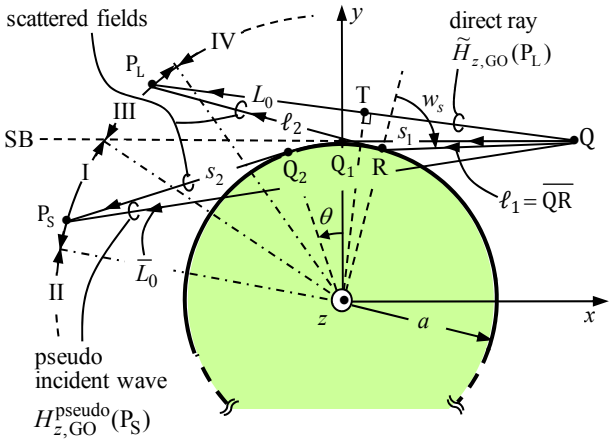

Fig. 2. Pseudo incident wave and scattered field observed at the point $\mathrm{P_S}$ located in the transition region I, and direct ray and scattered field observed at the point $\mathrm{P_L}$ located in the transition region III.

B. Asymptotic analysis in the deep shadow region II

We derive an asymptotic solution for the scattered field in the deep shadow region II as shown in Fig. 1.

When the $I(\xi, L)$ in (19) is performed by several manipulations, the following integral can be obtained.

$$I(\xi, L) = \frac{e^{-i\pi/4}}{2\sqrt{\pi}} \int_{C_0} \frac{w_2'(t)}{w_1'(t)} \exp\left[i\xi t + i\frac{M^2}{2kL}t^2\right] dt\,. \quad (24)$$

The pole singularities $t_m\,(m = 1, 2, 3, \cdots)$ are determined from the following characteristic equation:

$$w_1'(t_m) = 0\,, \quad m = 1, 2, 3, \cdots\,. \quad (25)$$

The integration contour C_0 in (24) is defined along the positive imaginary axis from $+i\infty$ to 0 and then along the positive real axis from 0 to $+\infty$ (see Fig. 2 in [12]). The integral in (24) can then be evaluated rigorously by applying the residue theorem. Substituting the above result of $I(\xi, L)$ into (1) and then performing the rearrangement yield the following surface diffracted ray solution for the scattered field effective also in the deep shadow region II comparatively near a conducting cylinder [9], [12].

$$H_z^d(\mathrm{P_S}) \sim H_{z,\mathrm{in}}(\mathrm{Q_1}) \sum_{m=1}^{\infty} \Big\{ D_m(\mathrm{Q_1}) A_m(\mathrm{Q_1}) \exp(ik\ell - \Omega_m \ell) \cdot D_m(\mathrm{Q_2}) A_m(\mathrm{Q_2}) \Big\} \frac{\exp(iks_2)}{\sqrt{s_2}}\,. \quad (26)$$

In (26), $H_{z,\mathrm{in}}(\mathrm{Q_1})$ denotes the incident cylindrical wave, $D_m(\mathrm{Q_1})(D_m(\mathrm{Q_2}))$ the GTD's surface diffraction coefficient at the point $\mathrm{Q_1}(\mathrm{Q_2})$, and Ω_m the attenuation constant for the mth creeping mode [3]. $A_m(\mathrm{Q_1})(A_m(\mathrm{Q_2}))$ is the new modification coefficient for $D_m(\mathrm{Q_1})(D_m(\mathrm{Q_2}))$ and can be obtained directly from the t^2 term in the exponential in (24).

The coefficients $D_m(\mathrm{Q_{1,2}})$, Ω_m, and $A_m(\mathrm{Q_{1,2}})$ are given by [9], [12] and the pole t_m is obtained from

$$t_m = \sigma_m e^{i\pi/3}\,, \quad Ai'(-\sigma_m) = 0. \quad (27)$$

C. Asymptotic analysis in the transition region III

We consider an asymptotic analysis for the scattered field in the transition region III as shown in Fig. 1.

Substituting $-|\theta|$ instead of θ in (20) and then applying the several approximations with $|\theta| \ll 1$, one may obtain the following asymptotic solution for the scattered field applicable in the transition region III [12].

$$H_z^d(\mathrm{P_L}) \sim \tilde{H}_{z,\,\mathrm{GO}}(\mathrm{P_L}) + H_{z,\mathrm{in}}(\mathrm{R}) B(k) \sqrt{\frac{\ell_1}{s_1 s_2}}\, e^{i\tilde{\xi}^3/12} \hat{P}_h^{\mathrm{ext}}(\tilde{\xi}, L) e^{ik\ell_2} \quad (28)$$

$$H_{z,\mathrm{in}}(\mathrm{R}) = \frac{i}{4}\sqrt{\frac{2}{\pi k \ell_1}} \exp\left[ik\ell_1 - i\frac{\pi}{4}\right],\ \ell_1 = \overline{\mathrm{QR}} \quad (29)$$

$$\tilde{\xi} = -M|\theta|\ (\leq 0). \quad (30)$$

The symbol (˜) is used for the solutions in the lit region. $\hat{P}_h^{\mathrm{ext}}(\tilde{\xi}, L)$ is the extended Pekeris caret function obtained by replacing ξ by $\tilde{\xi}$ in $\hat{P}_h^{\mathrm{ext}}(\xi, L)$ of (12). In (28), $\tilde{H}_{z,\,\mathrm{GO}}(\mathrm{P_L})$ is the direct ray passing through the turning point T and the second term of the right-hand side is a scattered field (see Fig. 2). $H_{z,\mathrm{in}}(\mathrm{R})$ is the incident cylindrical wave at the reflection point R and $\ell_1 (= \overline{\mathrm{QR}})$ is the propagation distance from the source Q to the point R and $\ell_2 (= \overline{\mathrm{RP_L}})$ from R to $\mathrm{P_L}$.

D. Asymptotic analysis in the deep lit region IV

Finally, we derive an asymptotic solution for the scattered field in the deep lit region IV as shown in Fig. 1.

Applying the saddle point technique into $\hat{P}_h^{\mathrm{ext}}(\tilde{\xi}, L)$ in (28) and then performing approximations with $|\theta| \ll 1$ yield the

following GO solution by the summation of the direct ray and the reflected geometrical ray effective in the deep lit region IV.

$$H_z^d(\mathrm{P_L}) \sim \widetilde{H}_{z,\,\mathrm{GO}}(\mathrm{P_L}) + H_{z,\mathrm{in}}(\mathrm{R})\Gamma_h \sqrt{\frac{\tilde{\rho}^\gamma}{\tilde{\rho}^\gamma + \ell_2}}\, e^{ik\ell_2}\,. \qquad (31)$$

Where $\Gamma_h(=1)$ is the reflection coefficient at the reflection point R. The square root term $\sqrt{\ }$ in (31) denotes the reflected ray divergence factor and can be obtained analytically since the extended Pekeris caret function $\hat{P}_h^{\mathrm{ext}}(\tilde{\xi}, L)$ in (28) to which the t^2 term in the argument of the exponential in the integrand is added was used. Notation $\tilde{\rho}^\gamma$ is the distance from the reflection point R to the caustic F and is defined by

$$\tilde{\rho}^\gamma = \overline{\mathrm{RF}} = \frac{\ell_1 a\cos w_s}{2\ell_1 + a\cos w_s}\,. \qquad (32)$$

IV. Numerical Results and Discussions

In this section, we perform the numerical calculations required to assess the validity of the various asymptotic solutions derived in Sec. III.

In Fig. 3, the scattered magnetic field magnitude curves are calculated as the function of the azimuthal angle $|\phi - \phi_0|$ when both the source Q and the observation point P are located relatively close to the cylindrical surface. Numerical parameters used in the calculations are given in the caption of Fig. 3. The SB is located at 95.7°. The numerical results of the exact solution from the eigenfunction expansion [5], [9], the asymptotic solution in (20), and the asymptotic solution in (28) are indicated by the solid curve (——), the open circles (○○○), and the closed circles (●●●), respectively. The closed squares (■■■) are the calculation results by the superposition of the surface diffracted ray solution in (26) for the counterclockwise direction ($\mathrm{Q} \to \mathrm{Q}_1 \curvearrowright \mathrm{Q}_2 \to \mathrm{P}$) and the surface diffracted ray solution for the clockwise direction ($\mathrm{Q} \to \mathrm{Q}_1' \curvearrowright \mathrm{Q}_2' \to \mathrm{P}$) shown in Fig. 1. Also, the broken curve (– – –) is the numerical result by the GO solution in (31) adding to the direct ray before passing through a turning point.

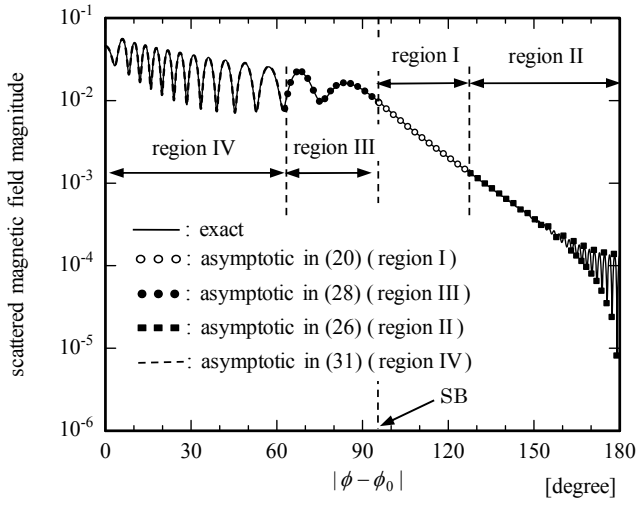

Fig. 3. Comparison between the various asymptotic solutions and the exact solution. Numerical parameters: $a = 5.0,\ \rho_0 = 8.0,\ \rho = 7.0$, and $ka = 100$.

It is confirmed that the asymptotic solutions of (20), (26), (28), and (31) agree excellently with the exact solution in the regions I, II, III, and IV, respectively (see Fig. 1).

V. Conclusion

We have derived the asymptotic solutions for the scattered field including the novel extended Pekeris caret function applicable in each of the transition regions divided by the SB into the shadow and the lit side when a cylindrical wave is incident on a conducting circular cylinder. We have also derived the surface diffracted ray solution and the geometrical optics solution which are effective exterior to the transition regions. By comparing with the exact solution, we have confirmed the validity of the various asymptotic solutions proposed in the present study.

Acknowledgment

The work was supported in part by the Grant-in-Aid for Scientific Research (C) (24560492) from Japan Society for the Promotion of Science (JSPS).

References

[1] J. B. Keller, "Diffraction by a convex cylinder," *IRE Trans. Antennas Propag.*, vol. 4, no. 3, pp. 312-321, July 1956.

[2] P. H. Pathak and R. G. Kouyoumjian, "An analysis of the radiation from apertures in curved surfaces by the geometrical theory of diffraction," *Proc. IEEE*, vol. 62, no. 11, pp. 1438-1447, Nov. 1974.

[3] P. H. Pathak, "An asymptotic analysis of the scattering of plane waves by a smooth convex cylinder," *Radio Sci.*, vol. 14, no. 3, pp. 419-435, May-June 1979.

[4] P. H. Pathak, W. D. Burnside, and R. J. Marhefka, "A uniform GTD analysis of the diffraction of electromagnetic waves by a smooth convex surface," *IEEE Trans. Antennas Propag.*, vol. 28, no. 9, pp. 631-642, Sept. 1980.

[5] G. L. James, Ed., *Geometrical Theory of Diffraction for Electromagnetic Waves*, 3rd ed., Chaps. 2-5, Peter Peregrinus, London, 1986.

[6] P. Hussar and R. Albus, "On the asymptotic frequency behavior of uniform GTD in the shadow region of a smooth convex surface," *IEEE Trans. Antennas Propag.*, vol. 39, no. 12, pp. 1672-1680, Dec. 1991.

[7] L. B. Felsen and N. Marcuvitz, Eds., *Radiation and Scattering of Wave*, Chap. 6, IEEE Press, New Jersey, 1994.

[8] K. Goto, T. Ishihara, and L. B. Felsen, "High-frequency (whispering-gallery mode) -to-beam conversion on a perfectly conducting concave-convex boundary," *IEEE Trans. Antennas Propag.*, vol. 50, no. 8, pp. 1109-1119, Aug. 2002.

[9] T. Ida and T. Ishihara, "Novel high-frequency uniform asymptotic solution for scattered field by a conducting cylinder," *IEICE Trans. Electron.* (Japanese Edition), vol. J87-C, no. 10, pp. 754- 767, Oct. 2004.

[10] N. A. Logan, Ed., General Research in Diffraction Theory, vol. 1, LMSD-288087, Missiles and Space Div., Lockheed Aircraft Corp., Sunnyvale, Calif., 1959.

[11] L. B. Felsen and N. Marcuvitz, Eds, *Radiation and Scattering of Waves*, Chap. 4, IEEE Press, New Jersey, 1994.

[12] K. Goto and L. H. Loc, "Asymptotic analysis for high-frequency scattered field by a conducting circular cylinder," *The Papers of Technical Meeting on EMT, IEE Japan,* EMT-12-148, pp. 161-166, Nov. 2012.

[13] M. Abramowitz and I. A. Stegun, Eds, *Handbook of Mathematical Functions*, pp. 358-478, Dover, New York, 1972.